Article

A General Nonaqueous Route to Binary Metal Oxide Nanocrystals Involving a C–C Bond Cleavage

Nicola Pinna, Georg Garnweitner, Markus Antonietti, and Markus Niederberger

J. Am. Chem. Soc., **2005**, 127 (15), 5608-5612• DOI: 10.1021/ja042323r • Publication Date (Web): 24 March 2005

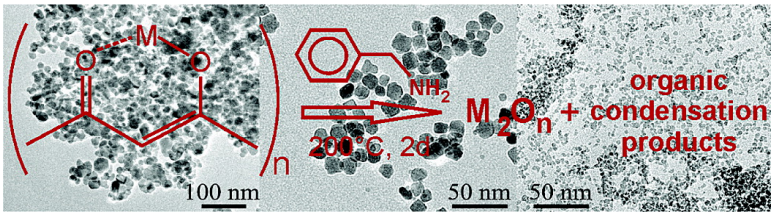

More About This Article

Additional resources and features associated with this article are available within the HTML version:

- Supporting Information
- Links to the 10 articles that cite this article, as of the time of this article download
- Access to high resolution figures
- Links to articles and content related to this article
- Copyright permission to reproduce figures and/or text from this article

View the Full Text HTML

J|A|C|S
ARTICLES
Published on Web 03/24/2005

A General Nonaqueous Route to Binary Metal Oxide Nanocrystals Involving a C−C Bond Cleavage

Nicola Pinna, Georg Garnweitner, Markus Antonietti, and Markus Niederberger*

Contribution from the Max Planck Institute of Colloids and Interfaces, Research Campus Golm, 14424 Potsdam, Germany

Received December 21, 2004; E-mail: markus.niederberger@mpikg.mpg.de

Abstract: A widely applicable solvothermal route to nanocrystalline iron, indium, gallium, and zinc oxide based on the reaction between the corresponding metal acetylacetonate as metal oxide precursor and benzylamine as solvent and reactant is presented. Detailed XRD, TEM, and Raman studies prove that, with the exception of the iron oxide system, where a mixture of the two phases magnetite and maghemite is formed, only phase pure materials are obtained, γ-Ga_2O_3, zincite ZnO, and cubic In_2O_3. The particle sizes lie in the range of 15−20 nm for the iron, 10−15 nm for the indium, 2.5−3.5 nm for gallium, and around 20 nm for zinc oxide. GC−MS analysis of the final reaction solution after removal of the nanoparticles showed that the composition is rather complex consisting of more than eight different organic compounds. Based on the fact that *N*-isopropylidenebenzylamine, 4-benzylamino-3-penten-2-one, and *N*-benzylacetamide were the main species found, we propose a detailed formation mechanism encompassing solvolysis of the acetylacetonate ligand, involving C−C bond cleavage, as well as ketimine and aldol-like condensation steps.

Introduction

The nonaqueous synthesis of oxidic compounds started decades ago, when investigations of Gerrard et al. on the interaction of alcohols with silicon tetrachloride gave evidence that this reaction resulted in the formation of hydrated silica and alkyl chlorides.[1] Many years later, related processes were applied to the preparation of monolithic silica[2] and metal oxide gels.[3] The extension of these nonhydrolytic reactions to the synthesis of titania nanocrystals[4] was a first step in opening up new pathways to a large variety of metal oxide nanoparticles such as iron oxides,[5] ZrO_2,[6] $HfO_2/Hf_xZr_{1-x}O_2$,[7] ZnO,[8] or ferrites.[9] Most of these procedures still rely on the use of surfactants such as trioctylphosphine oxide (TOPO) to control the crystal growth and to provide solubility. However, TOPO is toxic, leads to impurities in the final product, and hampers the application of these nanomaterials in electronic and sensing devices.

More advanced processes are based on the use of solvents, which act as reactant as well as control agent for particle growth, and thus allow the synthesis of high-purity nanomaterials. Another important point on the way to industrial scale-up is the generalization of a specific synthesis methodology, so that the same reaction setup can be used for as many different materials as possible. Regarding these requirements, the "benzyl alcohol route" is particularly versatile for the synthesis of diverse binary metal oxides,[10−15] perovskites,[16,17] and nanohybrid materials.[18] However, this approach is rather restricted, when metal alkoxides are either commercially not available or only at very high price, or when metal halide precursors are undesirable because of halide impurities in the final oxidic material.

To circumvent some of these drawbacks, we present in this work an alternative route to nanocrystalline iron, indium,

(1) Gerrard, W.; Woodhead, A. H. *J. Chem. Soc.* **1951**, 519.
(2) Corriu, R. J. P.; Leclercq, D.; Lefevre, P.; Mutin, P. H.; Vioux, A. *J. Non-Cryst. Solids* **1992**, *146*, 301.
(3) Corriu, R. J. P.; Leclercq, D.; Lefevre, P.; Mutin, P. H.; Vioux, A. *J. Mater. Chem.* **1992**, *2*, 673.
(4) Trentler, T. J.; Denler, T. E.; Bertone, J. F.; Agrawal, A.; Colvin, V. L. *J. Am. Chem. Soc.* **1999**, *121*, 1613.
(5) (a) Hyeon, T.; Lee, S. S.; Park, J.; Chung, Y.; Na, H. B. *J. Am. Chem. Soc.* **2001**, *123*, 12798. (b) Park, J.; An, K.; Hwang, Y.; Park, J. G.; Noh, H. J.; Kim, J. Y.; Park, J. H.; Hwang, N. M.; Hyeon, T. *Nat. Mater.* **2004**, *3*, 891. (c) Redl, F. X.; Black, C. T.; Papaefthymiou, G. C.; Sandstrom, R. L.; Yin, M.; Zeng, H.; Murray, C. B.; O'Brien, S. P. *J. Am. Chem. Soc.* **2004**, *126*, 14583.
(6) Joo, J.; Yu, T.; Kim, Y. W.; Park, H. M.; Wu, F. X.; Zhang, J. Z.; Hyeon, T. *J. Am. Chem. Soc.* **2003**, *125*, 6553.
(7) Tang, J.; Fabbri, J.; Robinson, R. D.; Zhu, Y. M.; Herman, I. P.; Steigerwald, M. L.; Brus, L. E. *Chem. Mater.* **2004**, *16*, 1336.
(8) (a) Shim, M.; Guyot-Sionnest, P. *J. Am. Chem. Soc.* **2001**, *123*, 11651. (b) Cozzoli, P. D.; Curri, M. L.; Agostiano, A.; Leo, G.; Lomascolo, M. *J. Phys. Chem. B* **2003**, *107*, 4756.
(9) (a) Sun, S.; Zeng, H.; Robinson, D. B.; Raoux, S.; Rice, P. M.; Wang, S. X.; Li, G. *J. Am. Chem. Soc.* **2004**, *126*, 273. (b) Zeng, H.; Rice, P. M.; Wang, S. X.; Sun, S. *J. Am. Chem. Soc.* **2004**, *126*, 11458.
(10) Niederberger, M.; Bartl, M. H.; Stucky, G. D. *J. Am. Chem. Soc.* **2002**, *124*, 13642.
(11) Niederberger, M.; Bartl, M. H.; Stucky, G. D. *Chem. Mater.* **2002**, *14*, 4364.
(12) Niederberger, M.; Garnweitner, G.; Krumeich, F.; Nesper, R.; Cölfen, H.; Antonietti, M. *Chem. Mater.* **2004**, *16*, 1202.
(13) Pinna, N.; Antonietti, M.; Niederberger, M. *Colloids Surf., A* **2004**, *250*, 211.
(14) Pinna, N.; Garnweitner, G.; Antonietti, M.; Niederberger, M. *Adv. Mater.* **2004**, *16*, 2196.
(15) Pinna, N.; Neri, G.; Antonietti, M.; Niederberger, M. *Angew. Chem., Int. Ed.* **2004**, *43*, 4345.
(16) Niederberger, M.; Pinna, N.; Polleux, J.; Antonietti, M. *Angew. Chem., Int. Ed.* **2004**, *43*, 2270.
(17) Niederberger, M.; Garnweitner, G.; Pinna, N.; Antonietti, M. *J. Am. Chem. Soc.* **2004**, *126*, 9120.
(18) Pinna, N.; Garnweitner, G.; Beato, P.; Niederberger, M.; Antonietti, M. *Small* **2005**, *1*, 112.

10.1021/ja042323r CCC: $30.25

gallium, and zinc oxide, based on the reaction between the corresponding metal acetylacetonate and benzylamine. In the case of the presented metal oxides, it is particularly advantageous for economic reasons to use acetylacetonates instead of metal alkoxides. The reaction between acetylacetonates and oleylamine has already been reported for the synthesis of indium and manganese oxide nanoparticles by Park et al.[19,20] The authors proposed that the particle formation involved the thermal decomposition of the acetylacetonate, but they did not provide any further details. While studying the mechanism, we found that nanoparticle formation proceeds via a novel pathway involving a C−C bond cleavage in the acetylacetone molecule. In principle, this observation is antagonistic to the formation mechanism found in the $BaTiO_3$ system, where a C−C bond formation occurred between benzyl alcohol and the 2-propanolate ligand.[17]

Experimental Details

Synthesis. All synthesis procedures were carried out in a glovebox (O_2 and H_2O <0.1 ppm). In a typical synthesis of nanoparticles, 1.0 g of $Fe(acac)_3$ (2.81 mmol), 0.5 g of $In(acac)_3$ (1.21 mmol), 0.5 g of $Ga(acac)_3$ (1.36 mmol), or 0.5 g of $Zn(acac)_2{\cdot}xH_2O$ (1.90 mmol), respectively, was added to 20 mL of benzylamine. The reaction mixture was transferred into a Teflon cup of 45 mL inner volume, slid into a steel autoclave, and carefully sealed. The autoclave was taken out of the glovebox and heated in a furnace at 200 °C for 2 days. The resulting milky suspensions were centrifuged, and the precipitates thoroughly washed with ethanol and dichloromethane and subsequently dried in air at 60 °C.

Characterization. For transmission electron microscopy (TEM) studies, one or more drops of the dispersion of the nanoparticles in ethanol were deposited on an amorphous carbon film. A Philips CM200 FEG microscope, 200 kV, equipped with a field emission gun was used. The coefficient of spherical aberration was C_s = 1.35 mm. X-ray powder diffraction (XRD) patterns of all samples were measured in reflection mode (Cu Kα radiation) on a Bruker D8 diffractometer equipped with a scintillation counter.

Raman spectra were measured in micro-Raman backscattering geometry. They were recorded using a HeNe-laser (632.8 nm, Melles Griot, 17 mW) for excitation. The laser light was focused onto the sample using a 100× objective lens (Olympus), and the backscattered Raman lines were detected on a CCD camera (1024 × 298 pixel), which was Peltier-cooled to 243 K to reduce thermal noise. The spectrometer was operated in the confocal mode setting the entrance slit to 200 μm and the confocal hole to 400 μm. A notch filter was applied, to cut off the laser line and the Rayleigh scattering up to ca. 150 cm^{-1}.

GC−MS analysis was carried out on a Varian Series 3400 gas chromatograph equipped with a fused-silica column (30 m × 0.25 mm i.d.) coated with a 0.25 μm film of DB5 poly(5% diphenyl-95% dimethylsiloxane) from J&W Scientific. The sample was diluted with chloroform in a volume ratio of 1:2 before the measurement (ca. 1 μL was injected). The injector temperature was 270 °C. The oven temperature was maintained isothermal at 50 °C for 1 min and then increased to 250 °C at a rate of 20 °C min^{-1}. The final temperature was held for 10 min. For assignment of the individual signals, the gas chromatograph was directly coupled to a SSQ 710 quadrupole MS by Finnigan. ^{1}H-BB-decoupled ^{13}C NMR measurements were performed on a Bruker DPX 400 spectrometer at 100 MHz, at a sample spinning rate of 20 Hz and with a ZG30 pulse program.

Results and Discussion

The powder X-ray diffraction (XRD) patterns of the as-synthesized metal oxide samples are shown in Figure 1. All diffraction peaks can be assigned to the respective phases without indication of other crystalline byproducts. The reflections of the In_2O_3 nanoparticles are sharp and correspond to the cubic structure (Figure 1, ····, JCPDS [6-416]). Gallium oxide (Figure 1, - - - -) exhibits broader peaks characteristic for small crystallite sizes with the γ-Ga_2O_3 structure (JCPDS [20-426]). The sharp reflections of the XRD pattern of zinc oxide (Figure 1, − − −) can be attributed to the zincite structure ZnO (JCPDS [36-1451]). The pattern of the iron oxide exhibits broad peaks (Figure 1, −) matching both the magnetite Fe_3O_4 (JCPDS [19-629]) and the maghemite γ-Fe_2O_3 (JCPDS [39-1346]) structures. The XRD patterns of magnetite and maghemite just differ in a few low intensity reflections (<5%) present at 2θ = 23.8° and 26.1°, and, therefore, Raman measurements have to be consulted to unambiguously assign the crystal phase.[21,22]

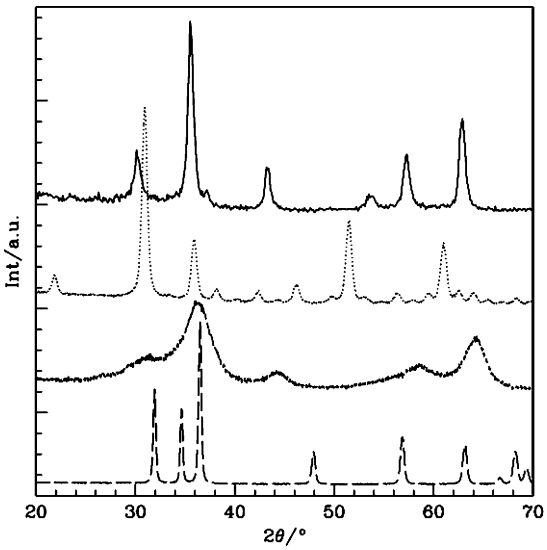

Figure 1. XRD patterns of the iron oxide (−), indium oxide (····), gallium oxide (- - - -), and zinc oxide (− − −) samples.

Figure 2 presents the Raman spectrum of the iron oxide nanoparticles. There is a main band at 672 cm^{-1}, which is characteristic for magnetite. The broad structures around 700, 500, and 350 cm^{-1}, respectively, are typical for maghemite[22] and give evidence that as a matter of fact the iron oxide sample consists of both phases.

Transmission electron microscopy (TEM) measurements of the as-synthesized particles are presented in Figure 3. The overview TEM image of the iron oxide particles (Figure 3a) shows that their size ranges from 15 to 20 nm. The maghemite phase as part of the iron oxide sample is further proved by the presence of the corresponding diffraction rings, as indicated by the arrows in Figure 3b. The indium oxide nanoparticles exhibit a cubic shape with sizes of 10−15 nm (Figure 3c), similar to In_2O_3 synthesized in benzyl alcohol.[15] As already expected from the XRD measurements, the gallium oxide nanoparticles are particularly small (Figure 3e), with sizes ranging from 2.5 to 3.5 nm. The zinc oxide displays less uniform particle morphology. In addition to spherical nanoparticles typically of 20 nm

(19) Seo, W. S.; Jo, H. H.; Lee, K.; Park, J. T. *Adv. Mater.* **2003**, *15*, 795.
(20) Seo, W. S.; Jo, H. H.; Lee, K.; Kim, B.; Oh, S. J.; Park, J. T. *Angew. Chem., Int. Ed.* **2004**, *43*, 1115.
(21) Cornell, R. M.; Schwertmann, U. *The Iron Oxides—Structure, Properties, Reactions, Occurrence and Uses*; VCH Verlagsgesellschaft: Weinheim, 1996.
(22) de Faria, D. L. A.; Venancio Silva, S.; de Oliveira, M. T. *J. Raman Spectrosc.* **1997**, *28*, 873.

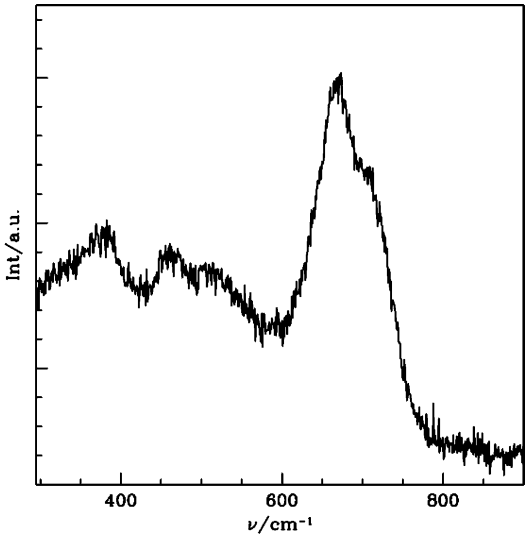

Figure 2. Raman spectrum of the iron oxide nanoparticles.

in diameter (Figure 3g), also nanorods were frequently found, generally about 200 nm long and 30 nm wide (Figure 3h). The crystal structure of these nanoparticles was additionally studied by selected area electron diffraction (SAED) as depicted in Figure 3b,d,f,i, respectively. In all cases, the patterns coincide well with the XRD data.

It is amazing that equal experimental conditions (i.e., the reaction of a metal acetylacetonate in benzylamine at 200 °C) lead to the formation of nicely crystalline nanopowders of different families of metal oxides. To investigate the formation mechanism for these systems, the composition of the obtained reaction solution was studied for each metal oxide after removal of the particles by centrifugation. The mixtures of organic reaction products found, however, turned out to be very similar for all systems. Therefore, only the iron oxide system will be discussed here in detail.

GC−MS analysis was performed to identify the components of the mixture, which was rather complex. Figure 4 shows the obtained chromatogram with individual peaks analyzed by MS (data not shown). $CHCl_3$ and other substances with low retention time are not shown in this plot. The largest peak (**1**) corresponds to the solvent benzylamine. A small amount of *N*-isopropylbenzylamine was also found (**2**), whereas the amount of *N*-isopropylidenebenzylamine was quite significant (**3**). Peak **4** is attributed to 4-benzylamino-3-penten-2-one, while **5** stems from *N*-benzylacetamide. Peak **6** is assigned to *N*-benzylidenebenzylamine, whereas peaks **7** and **8** are assumed to stem from *N*-(4-phenylbutan-2-ylidene)benzylamine and 5-benzylamino-1-phenyl-4-hexen-3-one, respectively. The small peaks (marked *) are attributed to other condensation products and are not discussed in detail due to their low quantity. The structures of the molecules are illustrated in Figure 5.

^1H and ^{13}C {^1H} NMR spectra basically confirm these results. The ^{13}C spectrum in Figure 6 shows, in addition to the excess of solvent (labeled S), the presence of substantial amounts of *N*-benzylacetamide (A) and, to a smaller extent, *N*-benzylidenebenzylamine (B). Significant amounts of acetone were also found in the mixture (C). *N*-Isopropylidenebenzylamine and *N*-isopropylbenzylamine were detected in small quantities, and *N*-(4-phenylbutan-2-ylidene)benzylamine as well as 5-benzylamino-1-phenyl-4-hexen-3-one were found in traces.

Catalysts such as hydrochloric acid are able to promote the alcoholysis of acetylacetone in alcohol to form acetone and acetic esters.[23] Under the influence of active metal centers such as yttrium, acetylacetone is cleaved even at room temperature.[24] The formation of acetic acid and acetone has also been found to occur during the formation of ZnO particles from Zn(II) acetylacetonate in a NaOH/EtOH mixture.[25] To the best of our knowledge, the analogous reaction of acetylacetone in amine solvents to form simple amides has not been described so far. However, the synthesis of *N*-benzylacetamide from 3-nitro-2,4-pentanedione has been reported.[26] As a reference experiment, we heated acetylacetone with benzylamine in an autoclave at 200 °C. No acetylacetone was left after this treatment, but substantial amounts of *N*-benzylacetamide were found. Therefore, the fact that the amide is present in the iron oxide reaction mixture in quite large amounts is seen as a solvolysis ("aminolysis") of acetylacetone and is not attributed to the formation of oxidic nanoparticles. During this process, no formal oxygen is released, which would be a requirement for the formation of Fe−O−Fe bonds. In the final reaction mixture, however, acetone is present to a far lower amount than *N*-benzylacetamide (molar ratio 0.2 acetone:1.0 amide, calculated from ^1H NMR measurements), although pro forma generated in stoichiometric amounts. This observation is attributed to further condensation of acetone, which has indeed been shown to constitute the key step in a novel nonaqueous pathway to metal oxides.[27,28]

For the system discussed here, we propose a combined solvolysis−condensation mechanism as illustrated in Scheme 1. Benzylamine nucleophilically attacks one carbonyl group of the acetylacetonate ligand (**1**). Aminolysis leads to *N*-benzylacetamide and an acetonate/enolate ligand coordinated to the iron center (**2**). Condensation between the acetonate and another benzylamine occurs via nucleophilic attack of the amine onto the electrophilic carbonyl center, leading to the release of a hydroxyl group (**3**) and the formation of an imine (**4**). The hydroxyl group bound to the Fe atom then induces condensation by attacking another iron center, resulting in the formation of an Fe−O−Fe bond. This step represents the starting point of crystallization. In principle, condensation of two hydroxyl groups would imply the concomitant elimination of water. Because the number of Fe−OH groups is small as compared to the amount of iron acetylacetonate, it is more probable that the condensation process takes place under elimination of acetylacetone via a nucleophilic attack of the OH oxygen to the monomeric iron species, and a proton transfer to the acetylacetone. This would render a truly nonhydrolytic formation process.

Although this mechanism is proposed as the main route, several other condensation products of acetone and benzylamine are observed. *N*-Benzylidenebenzylamine is formed by dehydrogenative oxidation of benzylamine and thus explains the formation of magnetite. Upon condensation of two benzylamine molecules under concurrent release of NH_3 (which is found when opening the autoclave), formally 1 mol of hydrogen is

(23) Adkins, H.; Kutz, W.; Coffman, D. D. *J. Am. Chem. Soc.* **1930**, *52*, 3212.
(24) Poncelet, O.; Hubert-Pfalzgraf, L. G. *Polyhedron* **1990**, *9*, 1305.
(25) Inubushi, Y.; Takami, R.; Iwasaki, M.; Tada, H.; Ito, S. *J. Colloid Interface Sci.* **1998**, *200*, 220.
(26) Tokumitsu, T.; Hayashi, T. *Nippon Kagaku Kaishi* **1983**, *1*, 88.
(27) Garnweitner, G.; Antonietti, M.; Niederberger, M. *Chem. Commun.* **2005**, 397.
(28) Goel, S. C.; Chiang, M. Y.; Gibbons, P. C.; Buhro, W. E. *Mater. Res. Soc. Symp. Proc.* **1992**, *271*, 3.

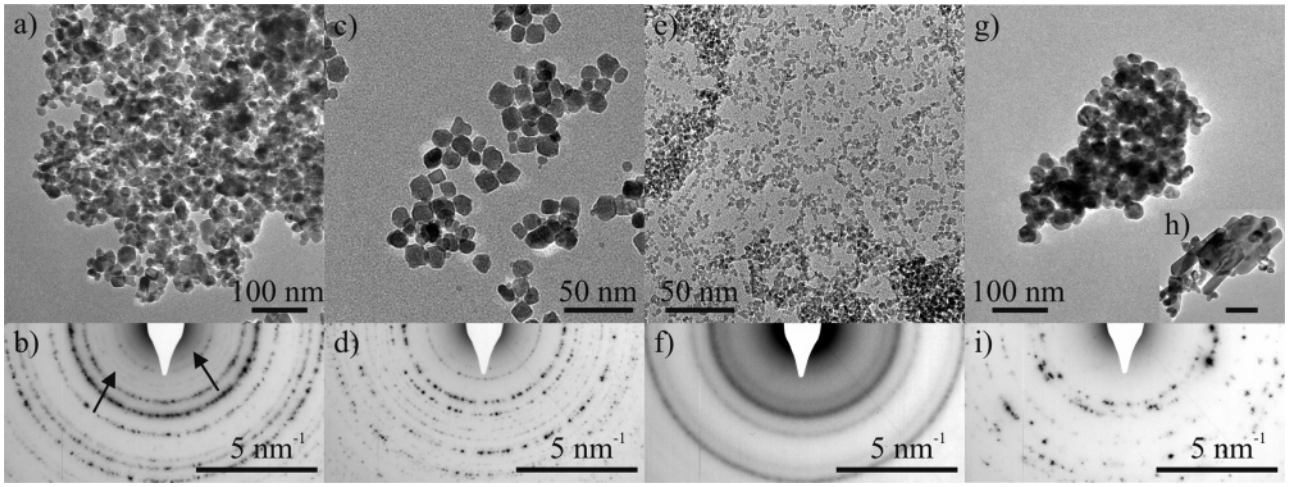

Figure 3. TEM overview images of (a) iron oxide, (c) indium oxide, (e) gallium oxide, and (g) and (h) zinc oxide nanoparticles (scale bar 100 nm) and their respective SAED patterns [b, d, f, and i].

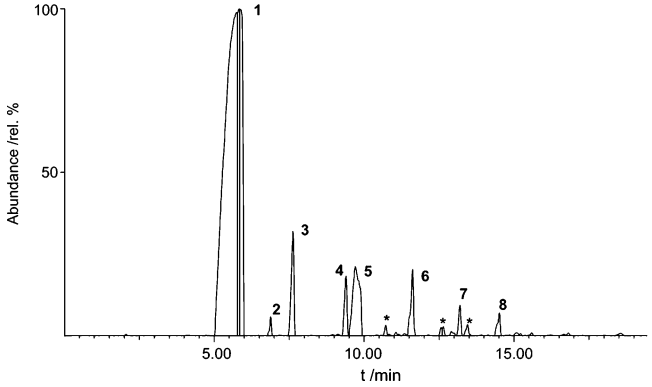

Figure 4. Gas chromatogram of the obtained reaction solution for the iron oxide system.

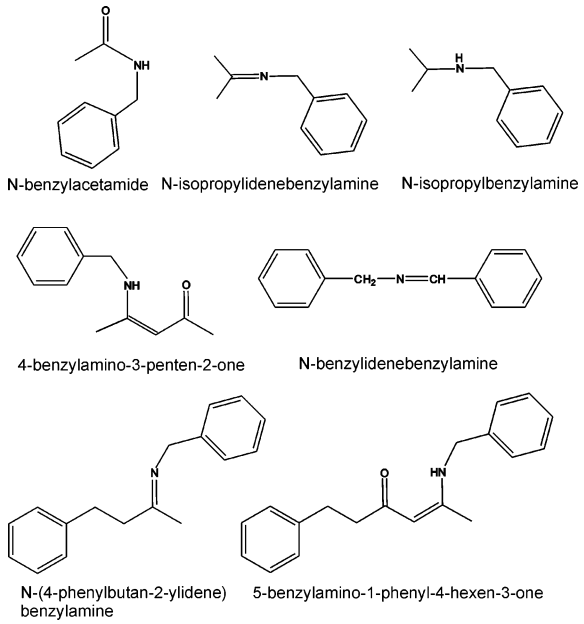

Figure 5. Structures of the organic species found in the final reaction mixture in the iron oxide system.

released, responsible for the reduction of the iron centers to Fe(II). As maghemite was also observed as a side product, it was not possible to relate the amount of *N*-benzylidenebenzylamine formed to the quantity of Fe(II) in the product.

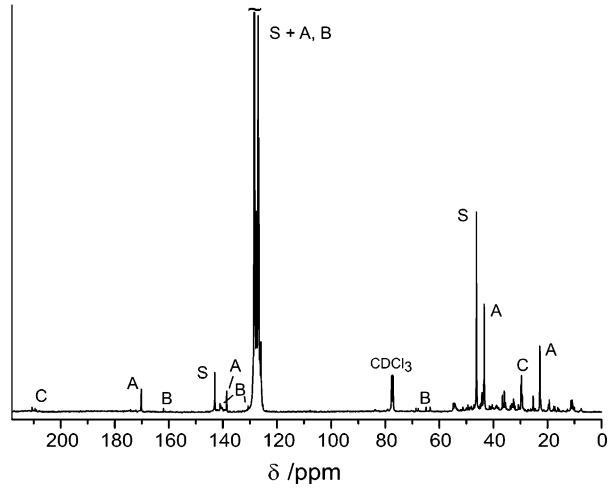

Figure 6. ^{13}C NMR spectrum of the final iron oxide reaction solution after particle removal.

Scheme 1. Proposed Pathway of the Reaction of Fe(III) Acetylacetonate in Benzylamine Leading to the Transfer of Oxygen to Iron To Enable Nanoparticle Formation

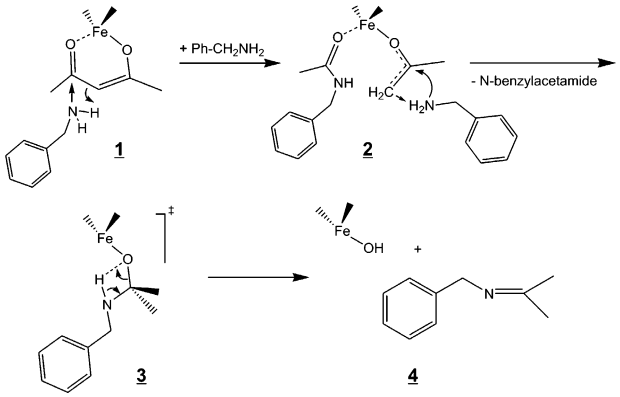

The presence of 4-benzylamino-3-penten-2-one, on the other hand, proves that not all acetylacetone is cleaved to form the amide. Instead, it can also directly undergo condensation (Scheme 2A). The reaction starts with the nucleophilic attack of benzylamine on one carbonyl center of the acetylacetonate (**1***). In contrast to the aminolysis, the C−C bond is not broken (**2***). The oxygen is released in the form of a hydroxyl group, (**3***), concurrently leading to 4-benzylamino-3-penten-2-one.

Scheme 2. Proposed Side Routes Additionally Occurring during the Formation of Iron Oxide Particles in Benzylamine

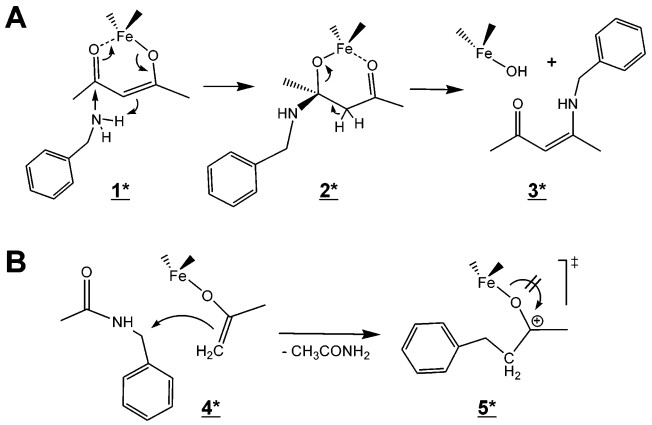

N-(4-Phenylbutan-2-ylidene)benzylamine and 5-benzylamino-1-phenyl-4-hexen-3-one are formed in an analogous fashion. The difference lies in a previous, additional coupling step of the enolate ligand with benzylamine, quite analogous to the aldol condensation steps described for the nanoparticle formation in ketones.[27] The suggested mechanism for this step is shown in Scheme 2B. The enolate ligand (formed during the main reaction, see Scheme 1) now acts as a nucleophile. As benzylamine is a good nucleophile itself, an attack of the amine is rather improbable. It is more likely that an amide is attacked (**4***), as the cleavage of benzyl groups from amide nitrogen is known to proceed under reasonably mild conditions.[29] This reaction would lead to the release of acetamide. However, acetamide was not found in the ^{13}C NMR spectrum, due to its low solubility in $CHCl_3$. An NMR measurement in D_2O (data not shown) revealed the presence of small amounts of acetamide, which supports this side mechanism. Because no water/hydroxide is formed in this step, the alkoxide is not released as the free ketone (**5***), but undergoes further condensation with benzylamine to form *N*-(4-phenylbutan-2-ylidene)benzylamine. Analogous reactions with uncleaved acetylacetonate would lead to 5-benzylamino-1-phenyl-4-hexen-3-one. It needs to be mentioned, however, that these side processes only take place to a small extent and therefore could not be thoroughly explored.

(29) Chern, C. Y.; Huang, Y. P.; Kan, W. M. *Tetrahedron Lett.* **2003**, *44*, 1039.

Conclusion

We showed that the use of metal acetylacetonates as monomeric precursor species for metal oxide formation together with benzylamine as a reactive solvent provides a comfortable and cheap route to binary metal oxide nanoparticles that are difficult to obtain via other nonaqueous synthesis routes. The as-synthesized powders are nanocrystalline and phase-pure. Only in the case of iron oxide, this synthesis approach leads to a mixture of two phases, magnetite and maghemite. The particle formation reaction proceeds via a novel pathway involving a cascade of reaction steps. Solvolysis of acetylacetone involving a C−C bond cleavage results in the formation of *N*-benzylacetamide and enolate ligands. The enolate ligands mainly undergo ketimine condensation reactions, which finally induce the formation of the metal oxide nanoparticles. A dehydrogenative oxidation of the solvent explains the partial formation of Fe(II), which is essential for the formation of magnetite.

Acknowledgment. We thank the Fritz-Haber-Institute and Prof. R. Schlögl for the use of the electron microscope, Klaus Weiss for technical assistance, and Pablo Beato for Raman measurements and fruitful discussions. Furthermore, we acknowledge Dr. I. Starke, University of Potsdam, for carrying out the GC−MS measurements.

JA042323R